J. Phys. Chem. Solids Vol. 43, No. 12, pp. 1129–1136, 1982
Printed in Great Britain.

0022-3697/82/121129-08$03.00/0
Pergamon Press Ltd.

STRUCTURE AND IONIC CONDUCTIVITY OF Bi_2O_3 SUBSTITUTED WITH LANTHANIDE OXIDES

M. J. VERKERK, G. M. H. VAN DE VELDE and A. J. BURGGRAAF
Twente University of Technology, Department of Chemical Engineering, Laboratory of Inorganic Materials Science, P.O. Box 217, 7500 AE Enschede, The Netherlands

and

R. B. HELMHOLDT
Netherlands Energy Research Foundation ECN, P.O. Box 1, 1755 ZG Petten, The Netherlands

(*Received* 1 *July* 1981; *accepted in revised form* 17 *February* 1982)

Abstract—A neutron diffraction study was performed on $(Bi_2O_3)_{0.80}(Er_2O_3)_{0.20}$ in the temperature region of 300–1100 K. There is no long-range ordering of vacancies. It is concluded from diffuse scattering that at low temperatures short-range ordering appears, leading to the occurrence of relatively short Ln-O distances. At temperatures above 870 K the oxygen lattice disorders.

In the low temperature region of Bi_2O_3–Ln_2O_3 solid solutions with the δ-Bi_2O_3 structure the activation energy of the conductivity is determined by the strength of the Ln–O band. In the high temperature region the energy necessary for oxygen ions to migrate through the tetrahedron planes plays a role.

1. INTRODUCTION

Bi_2O_3 was found to be an excellent oxygen ion conductor in the fluorite related δ-phase (fcc)[1]. This phase exists between 1002 K and the melting point at 1097 K[2]. By introduction of lanthanide oxides the highly ionic conductive phase (fcc) can be stabilized at low temperatures[3–7]. The conditions leading to the optimization of the conductivity in the Bi_2O_3–Ln_2O_3 systems have been described in[6]. The highest ionic conductivity is found in the Bi_2O_3–Er_2O_3 system for the sample containing 20 mole% Er_2O_3[5]. The conductivity of the stabilized bismuth sesquioxides is one decade or more higher than that of the stabilized zirconias.

In the stabilized bismuth sesquioxides with low substituent concentrations a decrease in the activation energy of the conductivity was observed at about 900 K. This change was correlated with an order–disorder transformation in the oxygen sublattice[6, 8]. To investigate this phenomenon we started a high-temperature neutron diffraction study on stabilized Bi_2O_3. The X-ray diffraction technique is of limited use in this case due to the small atomic form factor of oxygen.

A high-temperature neutron diffraction study on pure δ-Bi_2O_3 was performed by Harwig[9]. No long-range ordering was observed. It was proposed that each oxygen site in δ-Bi_2O_3 be replaced by four equivalent sites displaced in the ⟨111⟩ directions and that the oxygen ions occupy these sites statistically. Harwig[9] suggested that this model of the δ-Bi_2O_3 structure may be equivalent to a statistical description of a fluorite matrix containing ordered microdomains.

Neutron diffraction experiments on the structurally related stabilized zirconias (defect fluorite structure) were reported in[10–12]. Carter and Roth[10] concluded that the oxygen ions in calcia stabilized zirconia were displaced in the ⟨111⟩ direction. Steele and Fender[11] reported displacement of oxygen ions in the ⟨100⟩ direction for yttria and ytterbium stabilized zirconia. From diffuse scattering experiments they concluded that the vacancies are associated with lanthanide ions. Faber *et al.*[12] interpreted their measurements on calcia and yttria stabilized zirconia in terms of displacements of oxygen ions parallel and anti-parallel to the ⟨100⟩ direction, resulting in wave-like deformations of the oxygen lattice.

The object of this paper is to analyse ordering effects in stabilized Bi_2O_3 and to correlate these to the ionic conductivity.

2. EXPERIMENTAL PROCEDURES

2.1. *Preparation and characterization of the sample*

Bi_2O_3 containing 20.0 mole% Er_2O_3 was prepared by solid-state reaction. Bi_2O_3 (Merck, very pure) and Er_2O_3 (Serva, 99.9%) were thoroughly mixed and prefired at 1100 K for 16 hr and finely ground. The powder was poured into an alumina tube which was internally covered with a sheet of platinum. The sample was heated slowly to 1120 K, sintered for 72 hr and cooled down by $\frac{1}{2}$ K min^{-1}. The shrinkage of the rod permitted simple removal from the alumina tube. The density of the rod was about 90% of the theoretical density based on the defect fluorite-type lattice. The composition of the sample was checked using X-ray fluorescence with a method accuracy of 0.1% absolute. The amount of silicon and aluminium impurities was 0.008 and 0.03 wt% respectively. X-Ray diffraction showed sharp peaks (fcc) but no diffuse scattering was observed.

Conductivity measurements were generally not performed on the neutron diffraction samples, because the latter are porous and the former must be performed on dense ceramics. However, some of the conductivity measurements were performed on specimens which had

the same composition and the same thermal history as the neutron diffraction samples. See further Section 4.3.

2.2. *Neutron diffraction*

Neutron diffraction powder data have been collected at room temperature, 673, 773, 973 and 1073 K using the powder diffractometer at the HFR reactor at Petten. Neutrons of wavelength 2.5903 Å were obtained from the (111) planes of a copper crystal. Pyrolytic graphite with a thickness of 10 cm was employed[13] as a second order filter. Soller slits with a horizontal divergence of 30′ were placed between the reactor and monochromator and in front of each of the four ^{3}He counters. The sample was a rod having a length of 6 cm and a diameter of 1.1 cm placed within a cylindrical quartz ampoule filled with oxygen (10 Torr). The ampoule is described in[9]. To prevent contact between the sample and the quartz ampoule, platinum caps were fitted at the ends of the rod. As absorption of the sample was not negligible (μR = 0.797) the data were corrected for this effect.

Peaks due to diffuse scattering are usually transformed to a radial distribution function according to:

$$4\pi r^2(\rho(r)-\rho_0)=\frac{2r}{\pi}\int_0^\infty s\cdot i(s)\sin rs\,ds \qquad (1)$$

$\rho(r)$ is the atomic density as a function of the distance r, ρ_0 is the average atomic density of the sample, $s = (4\pi \sin\theta)/\lambda$, λ is the wavelength and θ is half the scattering angle, $i(s)$ is the normalized intensity corrected for the scattering of the average cell. Use of the Fourier inversion method requires good intensity data up to large values of $\sin\theta/\lambda$. Our preliminary diffuse scattering data did not permit us to carry out detailed calculations. The distances r_{ij} between pairs of atoms were calculated using a simplified equation:

$$\rho(r)=\frac{1}{r}\sum s\cdot i(s)\cdot\sin rs\cdot\Delta s. \qquad (2)$$

3. COMPILATION OF THE CONDUCTIVITY DATA

Figure 1 shows the Arrhenius plots of the conductivity of two samples in the Bi_2O_3–Er_2O_3 system. For the sample containing 20 mole% Er_2O_3 a bend is observed at T_B = 873 K. Below T_B the activation energy is (114.6 ± 0.5) kJ mole^{-1} and above the bend (62 ± 3) kJ mole^{-1}[5]. At a higher concentration of lanthanide, i.e. 35 mole% Er_2O_3, no bend in the Arrhenius plot is observed. This bend is also reported for Bi_2O_3 stabilized with other lanthanides at relatively low substituent concentrations[3, 4, 6, 7], for the lanthanide stabilized zirconias[14–17] and the lanthanide substituted cerias[18]. No changes in the symmetry or long-range ordering could be detected by X-ray diffraction techniques.

Figure 2 shows the activation energy E_a and pre-exponential factor σ_0 of the conductivity $\sigma(\sigma = \sigma_0 \exp -(E_a/RT))$ as a function of the composition x for lanthanide stabilized Bi_2O_3[3–6]. It appears that there are two different dependencies which can be related to

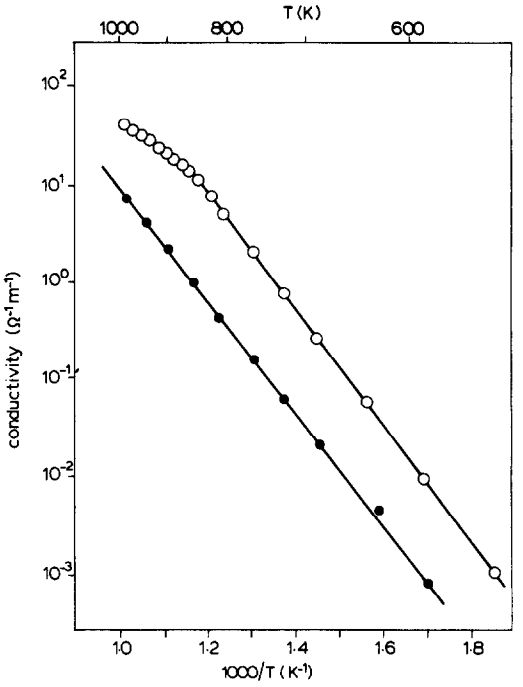

Fig. 1. Conductivity of $(Bi_2O_3)_{1-x}(Er_2O_3)_x$ in air. ○: $x = 0.20$; ●: $x = 0.35$.

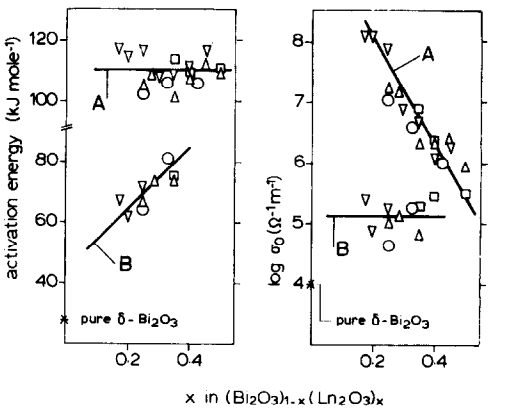

Fig. 2. The activation energy and log σ_0 of the Arrhenius plots of the conductivity for the $(Bi_2O_3)_{1-x}(Ln_2O_3)_x$ systems as a function of x. *A*: samples showing no bend in the Arrhenius plot and the low-temperature parts of the conductivity curve of samples showing a bend in the Arrhenius plot; *B*: high-temperature parts of the conductivity curve of samples showing a bend in the Arrhenius plot; ▽: Ln = Er; △: Ln = Dy; ○: Ln = Y; □: Ln = Gd.

different defect structures. For the high-temperature parts of the conductivity curve for samples showing a bend in the Arrhenius plot, E_a increases with increasing x whereas log σ_0 is independent of x (lines *B*). The values of E_a and log σ_0 extrapolated to $x = 0$ come close to the values of δ-Bi_2O_3. This suggests a defect structure analogous to δ-Bi_2O_3. For the samples showing no bend in the Arrhenius plot E_a is independent of x and log σ_0 decreases linearly with increasing x (lines *A*). For the samples showing a bend in the Arrhenius plot the same

holds for the low-temperature parts of the conductivity curve. This means a quite different defect structure compared to δ-Bi_2O_3. Previously the hypothesis was put forward[8] that in this region the oxygen ions are ordered and this will be further investigated and discussed (Sections 4 and 5).

In the low-temperature region there is a maximum in the conductivity of $(Bi_2O_3)_{1-x}(Ln_2O_3)_x$ at about $x = 0.20$–0.25 as shown for Ln = Er[5], Y and Yb[7]. Above T_B the conductivity decreases with increasing lanthanide content[3–7]. The conductivity of $(Bi_2O_3)_{0.65}(Ln_2O_3)_{0.35}$ increases with increasing ionic radius of the lanthanide[6].

4. NEUTRON DIFFRACTION OF $(Bi_2O_3)_{0.80}(Er_2O_3)_{0.20}$

4.1. *Models used for the neutron diffraction refinement*

For the refinements of the diffraction data of $(Bi_2O_3)_{0.80}(Er_2O_3)_{0.20}$ three models were evaluated: A: Sillén model; B: Gattow model; C: Willis model.

Sillén[19] reported a simple cubic phase for quenched Bi_2O_3 material, which must have been a Bi/Si mixed oxide in view of the preparation method. This simple cubic structure is related to the fluorite structure but has ordered defects in the oxygen sublattice in the ⟨111⟩ direction, as shown in Fig. 3(a). The Bi, Er atoms were placed in the (4c) position and the O atoms in the (6d) position of the space group Pn3m.

Gattow and Schröder[20] showed by means of high-temperature X-ray powder diffraction that the δ-phase of Bi_2O_3 has a cubic symmetry (fcc). They rejected an ordered defect oxygen lattice and gave preference to an oxygen sublattice with an average occupation of the sites (occupancy factor $\frac{3}{4}$), as shown in Fig. 3(b). The Bi, Er atoms were placed in the (4c) position and the O-atoms in the (8c) position of the space group *Fm3m*.

Willis[21, 22] replaced each anion in the fluorite structure by four equivalent sites displaced in the ⟨111⟩ direction from the position *xxx*, $x = \frac{1}{4}$ to *xxx*, $x = \frac{1}{4} + \delta$. The anions occupy these sites statistically (occupancy factor 3/16), see Fig. 3(c). The Bi, Er atoms were placed in the (4c) position and the O atoms in the (32f) position of the *Fm3m* space group. This model was applied to UO_2, ThO_2[21], CaF_2[22], $CeO_{1.79}$[23], $Ca_xZr_{1-x}O_{2-x}$($x = 0.1 \sim 0.2$) [10] and δ-Bi_2O_3[9]. This relaxation can be interpreted in two ways[21, 24]. In the first interpretation the fluorite structure is disordered, with some or all of the anions displaced in the ⟨111⟩ directions towards the octahedral holes at $\frac{1}{2}, \frac{1}{2}, \frac{1}{2}$. In the second interpretation the anion vibrates in an asymmetric anharmonic mode around the $\frac{1}{4}, \frac{1}{4}, \frac{1}{4}$ position towards the four octahedral holes. The second interpretation is generally favoured (Rouse, Willis and Pryor[24, 25]).

4.2. *Refinement of models*

The profile method[26] using the neutron diffraction data was applied for the refinement of the structure. The coherent scattering lengths used are $b(O) = 0.58$, $b(Bi) = 0.86$ and $b(Er) = 0.79 \times 10^{-14}$ m. The quantity χ_ν^2 given in the tables and figures is defined as: $\chi_\nu^2 = \Sigma\, W_i[Y_i(obs) - Y_i(calc)/k]^2/\nu$ where $Y_i(obs)$ and $Y_i(calc)$ are the observed and calculated intensities for the ith measured point, W_i its statistical weight, k the scale factor and ν the number of degrees of freedom.

At 300 K measurements were performed on two different samples. The relative intensities of the reflections were fairly reproducible. Figure 4 gives the neutron diffraction pattern at 773 K, together with the calculated profile. The peak at $2\theta = 23.4°$ is a $\lambda/2$ reflection of 111, the peak at $2\theta = 37°$ is caused by diffuse scattering from the quartz ampoule and the peaks at $2\theta = 66.7°$ and 72.5° are due to diffuse scattering from the sample. Peak shape parameters[26] were normal, no evidence for strain-broadened Bragg lines was found.

The measured lattice constant as a function of the

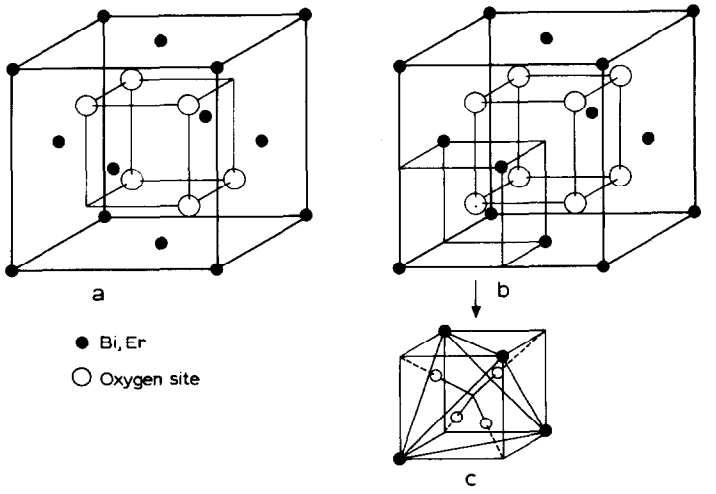

Fig. 3. Fluorite related structure models for $(Bi_2O_3)_{0.80}(Er_2O_3)_{0.20}$. (a) Sillén model: ordered defects in the ⟨111⟩ direction. (b) Gattow model: average distribution of 6 oxygen atoms about the (8c) sites of *Fm3m* (*xxx*, $x = \frac{1}{4}$). (c) Willis model: average distribution of 6 oxygen atoms about the (32*f*) sites of *Fm3m* (*xxx*, $x = \frac{1}{4} + \delta$). (after Harwig[37]).

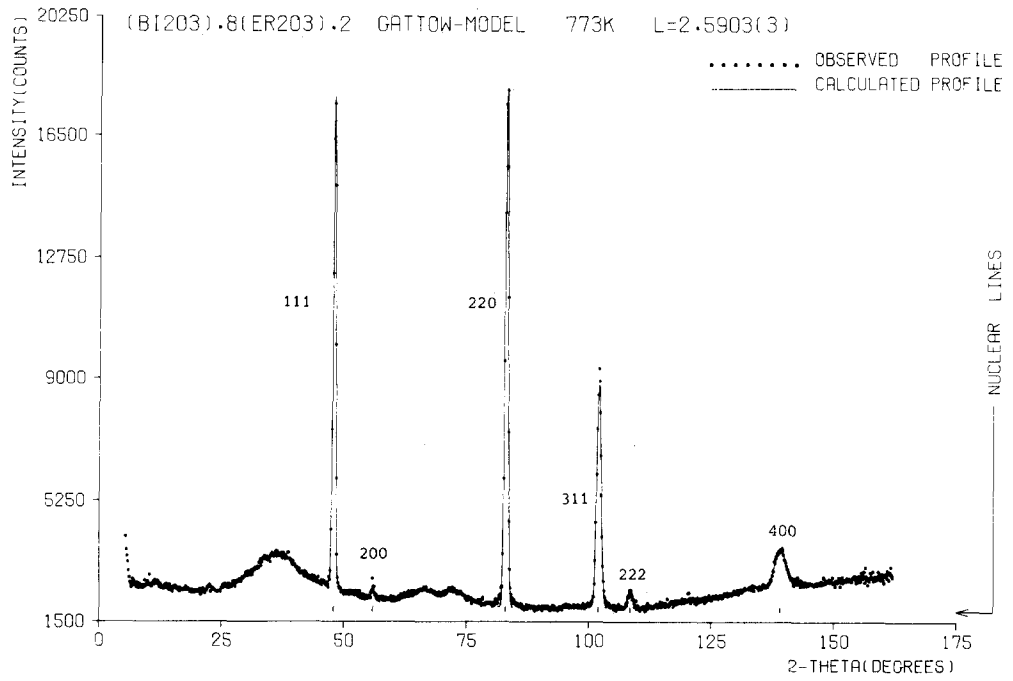

Fig. 4. Neutron diffraction profile of $(Bi_2O_3)_{0.80}(Er_2O_3)_{0.20}$ at 773 K.

temperature is given in Fig. 5. The broken line indicates the temperature of the bend in the Arrhenius plot (T_B). The neutron diffraction experiments suggest an increase of 0.17% in the lattice constant at T_B. This is confirmed by high-temperature Guinier experiments showing an increase of about 0.15%. At T_B there is also a strong increase in the expansion coefficient. It must be stressed again that no changes in the symmetry or long-range ordering could be observed.

Table 1 gives a survey of the results of the refinements and shows that χ_ν^2 for the Sillén model is not satisfactory. Long-range ordering of the oxygen vacancies in the ⟨111⟩ direction should be clearly indicated by the presence of the 110, 211, 310 and 321 reflections, which should have a significant intensity. These reflections are absent in our experimental data. We conclude that no long-range ordering of the oxygen vacancies appears in $(Bi_2O_3)_{0.80}(Er_2O_3)_{0.20}$.

Table 1 also gives the results of the refinement of the Gattow model. Below T_B the temperature factor of Bi, Er and O are temperature independent whereas above T_B they increase strongly with the temperature, see Table 1. It should be noticed that the temperature factors of Bi, Er and O are very high. Malros[27, 28] found at room temperature that for a single crystal of α-Bi_2O_3 $B_{Bi} \approx 0.6$ and $B_O \approx 1.0$.

Table 1 shows that the values of χ_ν^2 for the refinement of the Willis model are satisfactory. The Willis-parameter δ is not a function of temperature and is about 0.04. For δ-Bi_2O_3 at 1047 K Harwig[9] found $\delta = 0.066$. The χ_ν^2-value for the refinement of the Willis model is only slightly lower than the χ_ν^2-value for the refinement of the Gattow model. Using the Willis model there is one extra parameter. Applying Hamilton's test[30] to the χ_ν^2-values we found that on the basis of the χ_ν^2-values we cannot decide which of the two models is the better. When refining Harwig's[9] neutron diffraction data of δ-Bi_2O_3 (1047 K) we arrived at the same conclusion[31].

To evaluate the significance of the Willis parameter we investigated the sensitivity of χ_ν^2 and the temperature factors to changes in the values of the oxygen position. It appears that χ_ν^2 at 300 K is almost constant for $x = 0.21 \sim 0.30$ and at 1073 K for $x = 0.20 \sim 0.31 \cdot B_{Bi,Er}$ is practically constant over these ranges whereas B_O shows a parabolic dependence with the maximum at $x = 0.25$. However, the values of the temperature factors remain too high.

We also examined the possibility in which the oxygen vacancies cause displacements of cations and/or anions in the ⟨100⟩ directions[11, 12, 32, 33]. For oxygen ion displacements $B_{Bi,Er}$ is almost constant whereas B_O

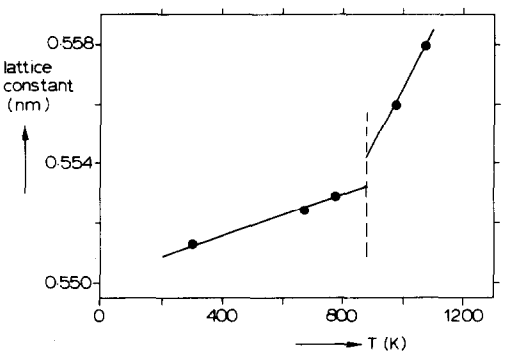

Fig. 5. Lattice constant of $(Bi_2O_3)_{0.80}(Er_2O_3)_{0.20}$ as a function of temperature measured by neutron diffraction. The broken line indicates the temperature of the bend in the Arrhenius plot.

Table 1. Refinement of $(Bi_2O_3)_{0.80}(Er_2O_3)_{0.20}$ for the Sillén model (A), Gattow model (B) and the Willis model (C). $B_{Bi,Er}$ and B_0 are the temperature factors for bismuth, erbium and oxygen respectively

T(K)	Model	$B_{Bi,Er}$(Å^2)	B_0(Å^2)	χ_ν^2	δ
300	A†	0.5(2)	10.9(5)	130	
	B	2.7(1)	11.6(2)	4.2	
	C	3.1(1)	7.5(5)	3.5	0.041(3)
673	B	3.1(1)	11.7(2)	3.8	
	C	3.6(1)	7.5(4)	3.2	0.041(3)
773	B	3.2(1)	11.9(2)	5.7	
	C	3.5(2)	8.9(8)	5.6	0.036(4)
973	B	4.1(1)	12.8(2)	2.7	
	C	4.8(2)	8.2(5)	2.3	0.043(2)
1073	B	4.9(1)	13.9(3)	3.6	
	C	5.3(3)	11(1)	3.5	0.037(6)

†This refinement was performed on diffraction data collected on a powdered sample in a steel holder.

shows a parabolic shape with a maximum at $x = 0.25$. For small displacements of cations $B_{Bi,Er}$ can decrease to reasonable values. These results may be an indication that there is a positional disorder in the cation sublattice or that the cations are displaced due to ordering. A more elaborate treatment of these displacement studies is given by Verkerk[31].

4.3. *Diffuse scattering*

Peaks due to diffuse scattering are observed in the neutron diffraction pattern, as shown in Fig. 4. The changes of these peaks with temperature is shown in Fig. 6. At temperatures above T_B the intensities of the peaks (corrected for background) decrease by at least a factor of two. At T_B the peak at 66.7° (2θ) shifts to 68.9° (2θ). The position of the second peak at 72° (2θ) scatters in the region 71–73° (2θ).

The data of Fig. 6 were reproducible: if several different specimens were cooled down slowly (0.5 K min^{-1}) from sinter temperature to room temperature, they showed the same diffuse diffraction spectrum. Due to experimental difficulties it could not be checked whether the phenomena were reversible during thermal cycling around 870 K. This is a point for future investigation. However, conductivity measurements on compositions having a "knee" in their conductivity/temperature curve show that this bend is reversible during thermal cycling without hysteresis. This suggests that the related ordering phenomena are reversible and consequently in our opinion the same holds for the diffuse scattering spectra.

The diffuse peaks are Fourier transformed according to eqn (2) and r_{ij}-values of about 2.77 Å are obtained. This agrees very well with the average O–O distance in $(Bi_2O_3)_{0.80}(Er_2O_3)_{0.20}$. When the peaks at 773 K are transformed separately r_{ij}-values are obtained of 2.68 Å and 2.90 Å.

For δ-Bi_2O_3 there is an increase in the background at about 68° (2θ). However, no peaks due to diffuse scattering are found (measurements of H. A. Harwig). Peaks due to diffuse scattering just before the 220 reflection are observed in many ionic conductors: ZrO_2-CaO[10], ZrO_2-Y_2O_3[11,35], ZrO_2-Yb_2O_3[11], $CeO_{1.79}$[34] and CaF_2-YF_3[36].

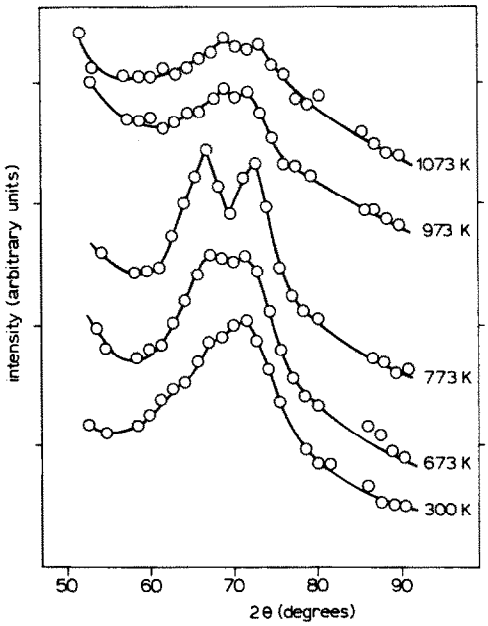

Fig. 6. Diffuse peaks of $(Bi_2O_3)_{0.80}(Er_2O_3)_{0.20}$ at different temperatures. Smoothed data: each point represents the average value of ten experimental points.

4.4. *Discussion*

The present results indicate a considerable positional disorder of the oxygen ions around the (8c) position and of the cations around the (4c) position or displacements of the ions due to ordering. The positional disorder or displacements of the ions are manifest as large temperature factors. On the basis of these results we can conclude that the *simplest* model to describe the structure of $(Bi_2O_3)_{0.80}(Er_2O_3)_{0.20}$ is the Gattow model in which the ions are positionally disordered or displaced due to ordering. The diffuse scattering results indicate a fluorite matrix containing short-range ordered units or ordered microdomains at low temperatures. This will be discussed now.

As has been stated before the r_{ij}-value of about 2.77 Å agrees very well with the calculated O–O distance in $(Bi_2O_3)_{0.80}(Er_2O_3)_{0.20}$. We calculated from the lattice constant at 773 K the following distances (Bi, Er)–O: 2.39 Å; O–O: 2.76 Å and (Bi, Er)–(Bi-Er): 3.91 Å. Analyzing the two peaks separately r_{ij}-values of 2.68 Å and 2.90 Å were obtained. It is quite probable that these values represent O–O distances. The distance 2.68 Å agrees well with the O–O distance in a hypothetical "fcc–Er_2O_3" in which the atoms are at the (8c) position. This O–O distance is calculated to be 2.64 Å at 773 K by extrapolation of the lattice constant of solid solutions of U_3O_8 and Er_2O_3 with the f.c.c. structure[38] to zero concentration of U_3O_8. The relevant expansion coefficient[39] has been used to calculate all data at the same temperature. This result means that the oxygen ions are displaced in the direction of an Er^{3+}-ion. Due to this displacement some O–O distances are decreased while others are increased as will be shown below.

On the basis of these results, together with some fundamental structural considerations a model of an ordered unit is proposed. In a highly defective structure a completely random arrangement of vacancies is unfavourable and is only possible in very small domains[40]. A part of the proposed model for the short range-ordered unit or ordered microdomains is given in Fig. 7. The size of the ordered units is unknown but must be very small because no superstructure reflections are observed in the diffraction pattern. In order to facilitate the discussion, the composition is taken to be $(Bi_2O_3)_{0.75}(Ln_2O_3)_{0.25}$. For this composition every tetrahedron consists of three Bi^{3+}-ions and one Ln^{3+}-ion and will be denoted as a (Bi_3, Ln)-tetrahedron. The cations are long-range ordered[41] by placing the lanthanide ions on the corners of the unit cell shown in Fig. 3(b) and the bismuth ions in the centre of the faces. Figure 7 shows the oxygen ions of a (001) plane at $Z = 3/4$. The cations above and below this plane are indicated. The oxygen ions are displaced in the direction of the lanthanide ions (Willis-type displacement with a negative δ towards a cation instead of a positive δ towards a vacancy). Ordering of vacancies is not relevant for our model but according to[29, 41] ordering in the ⟨111⟩ direction is most favourable. From Fig. 7 it is clear that two O–O distances have arisen. In the first place the O–O distance between the oxygen ions within an "fcc–Er_2O_3" unit, which has a value of 2.68 Å (measured r_{ij}-value) or 2.64 Å[38]. Secondly the O–O distance between the oxygen ions belonging to different units and calculated at 2.85 Å and 2.89 Å respectively. These values agree well with the measured r_{ij}-value of 2.90 Å. Further studies are necessary to confirm this ordering model and to distinguish between short-range order and ordered microdomains.

†The observed increase of the ionic conductivity of $(Bi_2O_3)_{0.65}(Ln_2O_3)_{0.35}$ with increasing ionic radius of the lanthanide must be ascribed to changes in E_a because σ_0 is constant. The strength of the Ln–O bond will decrease slightly with increasing ionic radius. From the conductivity data we calculated: $E_a(Ln = Gd) = 107$ kJ mole^{-1} and $E_a(Ln = Yb) = 111$ kJ mole^{-1}. This difference is too small to be measured.

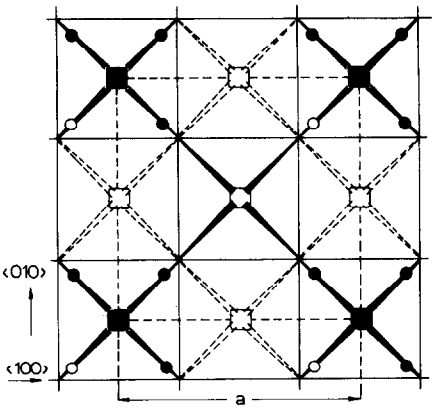

Fig. 7. A model of the ordered unit for $(Bi_2O_3)_{0.75}(Ln_2O_3)_{0.25}$. □: Bi^{3+}-ion; ■: Ln^{3+}-ion; ●: O^{2-}-ion; ○: O^{2-} vacancy. a = unit cell dimension (= 5.529 Å).

At temperatures above 873 K the intensity of the diffuse peaks decreases strongly. The lattice constant and the expansion coefficient increase due to disordering of the ordered units. The lattice behaves "δ-Bi_2O_3-like" in this temperature region, which is in accordance with the value of the expansion coefficient and with the electrochemical data (Sections 3 and 5).

5. RELATION BETWEEN STRUCTURE AND IONIC CONDUCTIVITY

In the proceeding section a model was proposed to account for the peaks due to diffuse scatering. The proposed model must explain the conductivity characteristics summarized in Section 3. The model proposed in Fig. 7 combined with two plausible assumptions gives a consistent qualitative explanation of the low temperature conductivity behaviour. This is summarized below and is further discussed in Sections 5.1 and 5.2. It is assumed that the activation energy of the conductivity is determined by the strength of the Ln–O bond and by the energy necessary to migrate through the tetrahedron planes. In the low-temperature region the first effect is predominant and in the high-temperature region the second effect also plays a role. In the low-temperature region only the oxygen ions in the (Bi_3, Ln)-tetrahedron are mobile and determine σ_0.

5.1. *Strength of the* Ln–O *bond and conductivity*

The Ln–O bond will be much stronger than the Bi–O bond because the stability of C-type Ln_2O_3, which is structurally related to defect fluorite is larger than that of Bi_2O_3. Also in the low-temperature region the Ln–O distance is shorter than the Bi–O distance due to ordering effects (see Fig. 7). Migration of an oxygen ion from one tetrahedron to the next empty one involves breaking of the Ln–O bond and passage through (Ln_2Bi), (Bi_2Ln) or Bi_3 tetrahedron planes.

It is assumed now that in the low-temperature region the activation energy will be mainly determined by the strength of this relatively short Ln–O bond. This strength will differ only slightly for the different lanthanides. Therefore, the activation energy of the conductivity is only slightly dependent on the lanthanide, as shown in Fig. 2.† As a consequence of this picture the activation

energy is determined by the strength of the short Ln–O bond in the (Bi_3, Ln)-tetrahedra and therefore will not change as a function of the lanthanide concentration as long as the (Bi_3, Ln) tetrahedra form a continuous network built up of (Bi_2Ln) and (Bi_3) tetrahedron planes. This is in accordance with the data in Fig. 2. (Bi_3, Ln) tetrahedra do play a crucial role in the low temperature region because only one single short Ln–O bond occurs. The oxygen-ions in the (Bi_2, Ln_2) tetrahedra are bonded to *two* lanthanide ions and for this reason hardly participate in the conductivity process. As can be seen in Fig. 7 the concentration of (Bi_3, Ln) tetrahedra has a maximum at 25 mole% lanthanide. Consequently an increase of the lanthanide concentration results in a decrease of the value of the pre-exponential factor σ_0 (the concentration of mobile oxygen ions) and of the conductivity, the activation energy being constant. The observed *linear* decrease of $\log \sigma_0$ with lanthanide concentration (Fig. 2) cannot be explained at present. Decreasing the lanthanide content (< 25 mole%) results in a decrease in the concentration of (Bi_3, Ln)-tetrahedra and an increase in the concentration of (Bi_4)-tetrahedra. In our opinion the oxygen ions in the (Bi_4)-tetrahedra do not take part in the conductivity process. In the low temperature region δ-Bi_2O_3 does not exist. Therefore the (Bi_4) tetrahedra will be distorted, probably to the rhombohedral or tetragonal distortion which occurs when the lanthanide content is less than the minimum concentration necessary to stabilize the fcc structure[3–7]. The fcc structure is locally destabilized and distorts locally to a lower symmetry from which is known that the conductivity is two decades or more lower than that of stabilized Bi_2O_3.

Consequently the conductivity has a maximum at the same lanthanide concentration where the (Bi_3Ln) concentration has a peak, i.e. at 25 mole% lanthanide. This is indeed observed[5].

At about 870 K the lattice disorders, resulting in an increase of the Ln–O distance. The strength of the Ln–O bond decreases and this results in a decrease of the activation energy. In the case of $(Bi_2O_3)_{0.80}(Er_2O_3)_{0.20}$ the Ln–O distance increases from 2.30 Å to 2.40 Å and the activation energy decreases by a factor of two, see Fig. 1. At high lanthanide concentration the activation energy is constant over the investigated temperature region, as shown for $(Bi_2O_3)_{0.65}(Er_2O_3)_{0.35}$ in Fig. 1. Hence, the relatively short Ln–O distance, belonging to the "fcc–Er_2O_3" unit, exists over the whole temperature region.

5.2. *Energy necessary to migrate through tetrahedron planes*

The total energy involved for the migration of an oxygen ion through a tetrahedron plane (E_m) consists of the Coulomb, repulsion, strain and polarization energies.

In the low-temperature region the activation energy is mainly determined by the strength of the Ln–O bond and E_m plays a minor role. In the high-temperature region all the oxygen ions take part in the conductivity process and there are no preferential diffusion paths. The experimentally observed activation energy increases with increasing lanthanide content, see Fig. 2. Two effects are important. First, the number of Ln–O bonds increases and secondly E_m increases due to a decrease of the contribution of the polarization energy. This can be concluded from the work of Demonchy *et al.*[42, 43]. They found that the activation energy of the conductivity of Bi_2O_3–PbO solid solutions at $T > 870$ K was equal to that of δ-Bi_2O_3, whereas the activation energy in the case of Bi_2O_3–SrO solid solutions increases with increasing SrO content. Now there is a large difference in polarizability between Pb^{2+} and Sr^{2+} ions: $\alpha(Pb^{2+}) = 3.6$ Å^3 and $\alpha(Sr^{2+}) = 0.9$ Å respectively [45]. The polarizability of Bi^{3+} is not well defined but can be estimated from the values for Tl^+(3.9 Å^3) and Pb^{2+}(3.6 Å^3), to be about 3.3 Å^3. This is comparable to that of Pb^{2+} and O^{2-}(3 Å^3).

Introduction of the less polarizable Sr^{2+} ion in a tetrahedron plane results in a *less negative* value of the polarization energy of the ensemble of cations with oxygen within this tetrahedron plane. Therefore, the energy during passage through the tetrahedron plane is increased. This results in a higher activation energy. The polarizabilities of Gd^{3+}–Yb^{3+} are in the region (1.01–0.80) Å^3[46] and are comparable with Sr^{2+}. Therefore, introduction of the less polarizable lanthanides in the bismuth sesquioxide lattice increases the value of E_m and, consequently, the activation energy. Detailed calculations are necessary to decide whether the strength of the Ln–O bond or the energy to migrate through a tetrahedron plane is predominant.

CONCLUSIONS

(1) The structure of $(Bi_2O_3)_{0.80}(Er_2O_3)_{0.20}$ was investigated by neutron diffraction in the region of 300–1100 K. It was concluded that no long-range ordering of vacancies appears. On the basis of the profile refinements no choice could be made between the Gattow and the Willis model. The anions and cations are positionally disordered or displaced due to ordering.

(2) It was concluded from diffuse scattering that at low temperatures two types of O–O distances are present (2.68 Å and 2.90 Å respectively). This leads to an ordering model in which oxygen ions are displaced towards the Ln^{3+}-ions (Willis-type displacement with a negative δ). At temperatures above 870 K the lattice disorders.

(3) A model was developed for the conductivity σ in the Bi_2O_3–Ln_2O_3 systems by combining the conductivity and the neutron diffraction results. This model explains the dependence of σ on composition, type of lanthanide and temperature. Its main features are summarized below. In the low-temperature region the activation energy of the conductivity is determined by the concentration of (Bi_3, Ln)-tetrahedra. In the high-temperature region the lattice disorders and all oxygen ions take part in the conductivity process, showing that σ_0 is constant. The activation energy of the conductivity is determined by the strength of the Ln–O bond and the energy necessary to migrate through the tetrahedron planes.

Acknowledgements—The authors are indebted to Dr. ir. T. van Dijk and Dr. S. Harkema for the stimulating discussions. Thanks are due to Mr. J. F. Strang for collection of neutron diffraction data. One of the authors (M.J.V.) acknowledges the financial assistance from Philips N. V. (Elcoma).

REFERENCES

1. Harwig H. A. and Gerards A. G., *J. Solid St. Chem.* **26**, 265 (1978).
2. Harwig H. A. and Gerards A. G., *Thermochimica Acta* **28**, 121 (1979).
3. Takahashi T., Iwahara H. and Arao T., *J. Appl. Electrochem.* **5**, 187 (1975).
4. Takahashi T., Esaka T. and Iwahara H., *J. Appl. Electrochem.* **7**, 31 (1977).
5. Verkerk M. J., Keizer K. and Burggraaf A. J., *J. Appl. Electrochem.* **10**, 81 (1980).
6. Verkerk M. J. and Burggraaf A. J., *J. Electrochem. Soc.* **128**, 75 (1981).
7. Cahen H. T., Thesis, State University Utrecht, 1980.
8. Verkerk M. J. and Burggraaf A. J., *Solid St. Ionics* **3**, 463 (1981).
9. Harwig H. A., *Z. Anorg. Allg. Chem.* **444**, 151 (1978).
10. Carter R. E. and Roth W. L., *EMF Measurements in High-Temperature Systems* (Edited by C. B. Alcock), Institute of Mining and Metallurgy, London (1968).
11. Steele D. and Fender B. E. F., *J. Phys. C.* **7**, 1 (1974).
12. Faber J. jr., Mueller M. H. and Cooper B. R., *Phys. Rev. B.* **17**, 4884 (1978).
13. Bergsma J. and Van Dijk C., *Nucl. Instr. Methods* **51**, 121 (1967).
14. Schouler E., Thesis, Grenoble, 1979.
15. Bernard H., Thesis, Grenoble, 1980.
16. Bauerle J. E. and Hrizo J., *J. Phys. Chem. Solids* **30**, 565 (1969).
17. Verkerk M. J., Middelhuis B. J. and Burggraaf A. J., *Solid St. Ionics* **6**, 159 (1982).
18. Kudo T. and Obayashi H., *J. Electrochem. Soc.* **122**, 142 (1975).
19. Sillén L. G., *Ark. Kemi Mineral. Geol.* **12A**, 1 (1937).
20. Gattow G. and Schröder H., *Z. Anorg. Allg. Chem.* **318**, 176 (1962).
21. Willis B. T. M., *Proc. Roy. Soc.* **A274**, 134 (1963).
22. Willis B. T. M., *Acta Cryst.* **18**, 75 (1965).
23. Faber J., Seitz M. A. and Müller M. H., *J. Chem. Phys. Solids* **37**, 903 (1976).
24. Wills B. T. M. and Pryor A. W., *Thermal Vibrations in Crystallography*, p. 168. Cambridge University Press (1975).
25. Rouse K. D., Willis B. T. M. and Pryor A. W., *Acta Cryst.* **B24**, 117 (1968).
26. Rietveld H. M., *J. Appl. Cryst.* **2**, 65 (1969).
27. Malmros G., *Acta Chem. Scand.* **24**, 384 (1970).
28. Malmros G. and Thomas J. O., *J. Appl. Cryst.* **10**, 7 (1977).
29. Harwig H. A. and Weenk J. W., *Z. Anorg. Allg. Chem.* **444**, 167 (1978).
30. Hamilton W. C., *Acta Cryst.* **18**, 502 (1965).
31. Verkerk M. J., Thesis, Twente University of Technology (1982).
32. Morinaga M., Cohen J. B. and Faber J. jr., *Acta Cryst.* **A35**, 789 (1979).
33. Morinaga M., Cohen J. B. and Faber J. jr., *Acta Cryst.* **A36**, 520 (1980).
34. Faber J., Seitz M. A. and Müller M. H., *J. Phys. Chem. Solids* **37**, 909 (1976).
35. Fender B. E. F., *Chemical Applications of Thermal Neutron Scattering* (Edited by Willis B. T. M.), p. 250. Oxford University Press (1973).
36. Willis B. T. M., *The Chemistry of Extended Defects in Non-metallic Solids* (Edited by L. Eyring and M. O'Keeffe). North-Holland, Amsterdam (1970).
37. Harwig H. A., Thesis, State University Utrecht, 1977.
38. Hund F. and Peetz U., *Z. Anorg. Allg. Chem.* **267**, 189 (1951).
39. *Gmelin, Handbuch der Anorg. Chemie*, Vol. **39**, Part C1 pp. 123–130. Verlag Chemie, Weinheim (1974).
40. Barker W. W., Graham J., Parks T. C. and Speed T. P., *J. Solid St. Chem.* **22**, 321 (1977).
41. Barker W. W. and Knop O., *Proc. Br. Cer. Soc.* **19**, 15 (1971).
42. Demonchy P., Conflant D., Boivin J. C. and Thomas D., *C. R. Acad. Sci. Ser. C* **289**, 317 (1979).
43. Demonchy P., Boivin J. C. and Thomas D., *C. R. Acad. Sci. Ser. C* **290**, 279 (1980).
44. Shannon R. D. and Prewitt C. T., *Acta Cryst.* **B25**, 925 (1969).
45. Phillips C. S. G. and Williams R. J. P., *Inorganic Chemistry (Part I)*, p. 176. Oxford (1965).
46. Gmelin, *Handbuch der Anorg. Chemie*, Vol. **39**, Part 4B, p. 125. Verlag Chemie, Weinheim (1976).